The International Journal of Advanced Manufacturing Technology (2018) 95:2379–2391
https://doi.org/10.1007/s00170-017-1411-x

ORIGINAL ARTICLE

The effect of friction stir processing and post-aging treatment on fatigue behavior of Ca-added flame-resistant magnesium alloy

Angga Afrinaldi[1] · Toshifumi Kakiuchi[2] · Ren Itoh[3] · Yoshiki Mizutani[4] · Yoshihiko Uematsu[2]

Received: 14 August 2017 / Accepted: 14 November 2017 / Published online: 23 November 2017

Abstract
Friction stir processing (FSP) was applied to the microstructural modification of the extruded flame-resistant magnesium (Mg) alloy, AMX602. The as-received material exhibited microstructure, in which intermetallic compounds (IMCs) were inhomogeneously dispersed in the matrix. FSP broke up some large IMCs and resulted in homogeneous distribution of IMCs and fine grains of the matrix. The micro hardness of the FSPed material was lower than that of the as-received one because the dislocation density and hardening precipitates decreased due to the heat input during FSP. The hardness of the FSPed material increased by the post-aging treatment. However, the fatigue strengths of the FSPed and post-aged specimens were lower than those of the as-received ones. The lower fatigue strengths of the FSPed specimens were attributed to the decrease of hardness by FSP. EBSD analyses revealed that strong texture was developed by FSP. The fatigue cracks of the post-aged specimens initiated at the locations with strong texture, in which basal slip planes had an angle about 45° to the fatigue loading direction. The lower fatigue strengths in the post-aged specimens were attributed to the texture-induced fatigue crack initiation mechanism.

Keywords Fatigue · Friction stir processing · Flame-resistant magnesium alloy · Microstructural modification · Texture

1 Introduction

Low gas emission and low fuel consumption are highly required in the field of engineering, particularly in the transporting vehicle machines such as airplanes and automobiles. The use of materials with light weight and high specific strength is one of the methods to achieve these requirements. Magnesium (Mg) alloys have light weight and high specific strength, and therefore, they are expected to be used widely for structural components in transportation systems [1]. On the other hand, the current applications of Mg alloys are limited because they have some disadvantages such as high combustibility, poor formability and relatively lower fatigue strengths than the other light weight alloys. Recently, some Mg alloys have been developed by adding calcium (Ca) element to decrease combustibility [2, 3]. Adding Ca increases the ignition temperature of Mg alloys as Ca makes stable oxides. However, some intermetallic compounds (IMCs) derived from the added Ca would be generated in the matrix [4]. To use those alloys for mechanical components, it is important to understand their fatigue properties in detail; thus, there have been a few studies on the fatigue behavior of the flame-resistant Mg alloys [5–7]. Masaki et al. [6] reported that Ca-based inclusions such as Al_2Ca with the size of 10 μm were found in Ca-added Mg alloy AMCa602, but fatigue cracks predominantly initiated from larger inclusions such as alumina nitride. Sakai et al. [7] reported that Ca-based inclusions played a role as the fatigue crack starter in AMCa602. Consequently, it can be assumed that such IMCs have detrimental effects on the fatigue behavior of flame-resistant Mg alloys.

Recently, friction stir processing (FSP) has been developed [8] as an application of friction stir welding (FSW), which could modify microstructures of materials by eliminating defects and inclusions and refining grains in Al alloys [9–12] and Mg alloys [13–16]. FSP is believed to be one of the

✉ Yoshihiko Uematsu
yuematsu@gifu-u.ac.jp

[1] Graduate School of Engineering, Gifu University, 1-1 Yanagido, Gifu 501-1193, Japan

[2] Department of Mechanical Engineering, Gifu University, 1-1 Yanagido, Gifu 501-1193, Japan

[3] Nabtesco Corporation, 7-9-2 Hirakawa-cho, Chiyoda-ku, Tokyo 102-0093, Japan

[4] Industrial Research Institute of Gifu Prefecture, 1288 Oze, Seki, Gifu 501-3265, Japan

Table 1 Chemical composition of AMX602 (wt.%)

Material	Al	Mn	Ca	Zn	Si	Cu	Fe	Ni	Mg
AMX602	5.82	0.27	2.06	< 0.001	< 0.01	< 0.001	< 0.001	< 0.001	Bal.

effective methods for improving mechanical properties and fatigue behavior [12, 15] by microstructural modification. However, there have been limited studies about the effect of FSP on the fatigue behavior of Mg alloys [15]. Furthermore, the effect of FSP on flame-resistant Mg alloys is not understood. In this study, FSP was applied to the flame-resistant Mg alloy AMX602, and the effect of FSP on the fatigue behavior was discussed based on the hardness, microstructures, crack initiation and fracture surface analyses. Furthermore, to understand the effect of FSP in detail, it is important to investigate the effect of texture developed during FSP because strong texture is frequently formed by sever plastic deformation in Mg alloys [17–19]. Thus, electron back scattered diffraction (EBSD) analyses were performed to investigate the effect of texture on fatigue behavior.

2 Material and experimental procedure

2.1 Material and specimen

The material used in this study is the extruded flame-resistant Mg alloy, AMX602, plate with the thickness of 5 mm. The chemical composition (wt.%) of the material is shown in Table 1. The as-received plates were FSPed under the conditions as will be described in the next section. Post-aging treatment was performed on some FSPed plates at 453 K (180 °C) for 40 h, and hereafter, the post-aged specimens are denoted as FSP/aged ones. Test specimens were machined from the as-received, FSPed and FSP/aged plates. The configurations of fatigue test specimens are shown in Fig. 1. Figure 1a is the standard type specimen with the gauge length of 12 mm, width of 6 mm, and thickness of 2.5 mm. The specimens with a narrow gauge width of 2 mm (Fig. 1b) were also used to examine the effect of the locally increased hardness and texture by FSP on the fatigue strength as would be described in Section 4. The FSPed and FSP/aged specimens were sampled from the plates, in which the longitudinal direction was parallel to the FSP tool traveling direction and the center of the specimen corresponded to the center of the tool path. Before fatigue tests, the surface of the gauge section was polished using #2000 grade emery paper and finally buff-finished into a mirror surface.

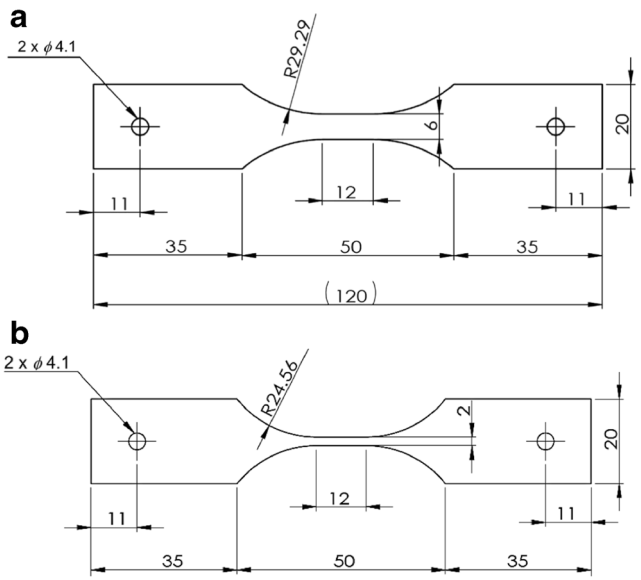

Fig. 1 Configuration of fatigue test specimen (thickness is 2.5 mm). **a** Standard type (Referred to Japanese Industrial Standard (JIS) Z 2275). **b** Narrow type with the gauge width of 2 mm

The FSP tool used in the present study has a concave shoulder with the diameter of 18.5 mm and an M8-threaded probe with the length of 4.7 mm. The tool was rotated clockwise and tilted 3° opposite to the FSP direction during the process. The tool traveling and rotational speeds were set at 300 mm/min and 800 rpm, respectively.

2.2 Experimental procedure

For the microstructural observation, the specimen surface was etched using the solution of picric acid 10 g, acetic anhydride 20 mL, ethanol 100 mL, and distilled water 20 mL. The chemical composition of the matrix and IMCs was analyzed using an energy-dispersive X-ray spectrometer (EDS). Fatigue tests were performed by an electro-hydraulic fatigue testing machine with the capacity of 98 kN. The fatigue loading waveform was sinusoidal with the test frequency, $f = 10$ Hz and stress ratio, $R = -1$. Hardness was measured using a micro Vickers hardness tester with a load of 0.98 N and dwell time of 30 s.

3 Results

3.1 Microstructural characterization

3.1.1 As-received material

Figure 2a, b, c is the microstructures of the as-received material observed on the planes perpendicular to the rolling

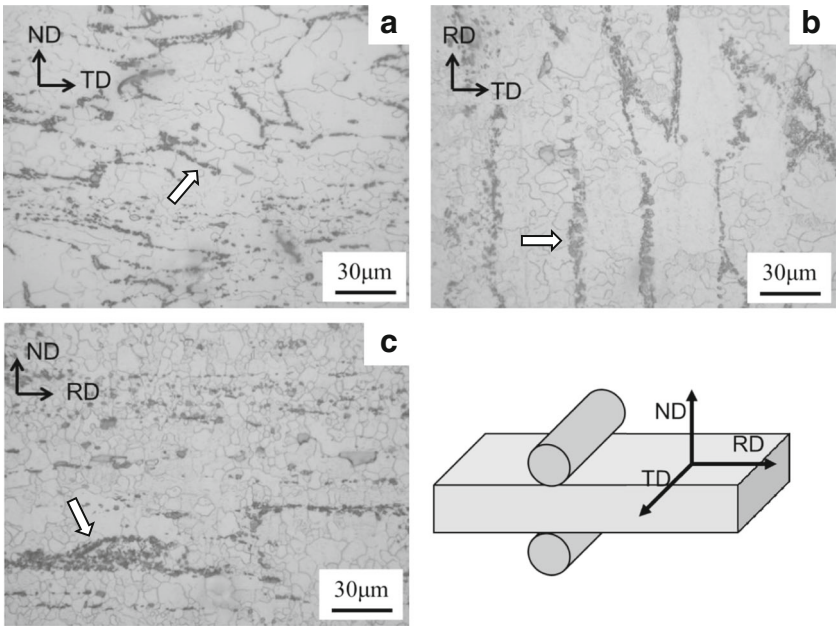

Fig. 2 Microstructures of the as-received material: Planes perpendicular to **a** rolling direction, **b** normal direction, and **c** transverse direction

direction (RD), normal direction (ND), and transverse direction (TD), respectively. The microstructure consists of equiaxed grains of α-Mg with the average grain size of 10.5 μm. IMCs are dispersed in the matrix as indicated by the arrows in the figures. It should be noted that the distribution of IMCs is not homogeneous depending on the rolling

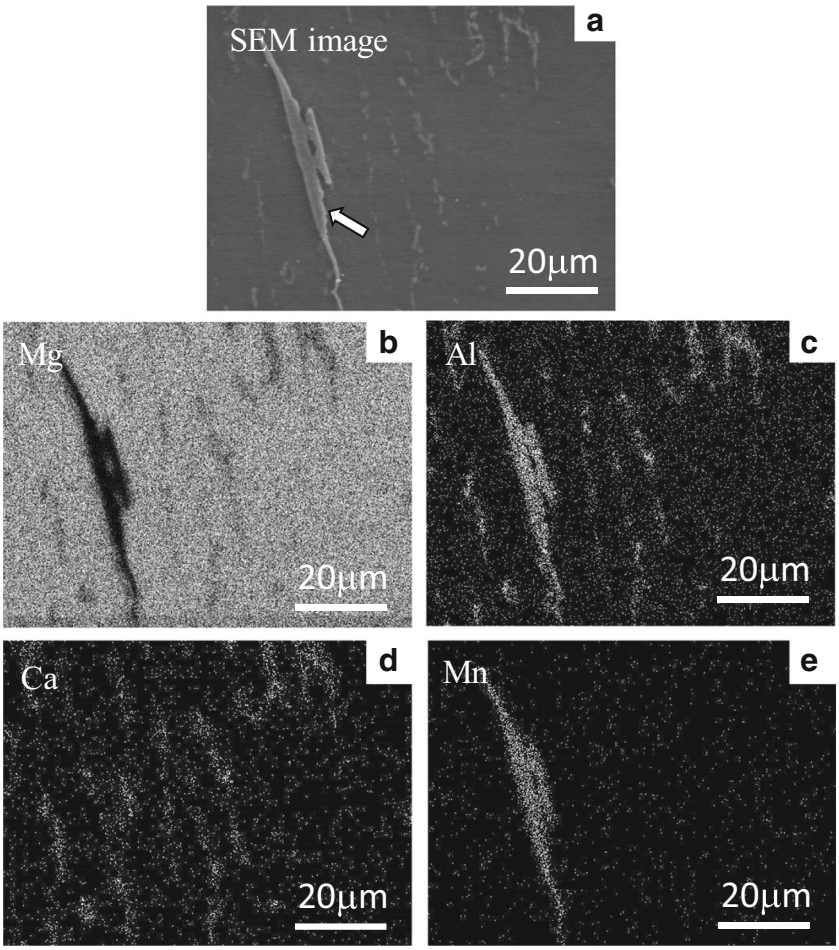

Fig. 3 SEM-EDS mapping of the as-received material: **a** SEM image, **b** Mg, **c** Al, **d** Ca, **e** Mn

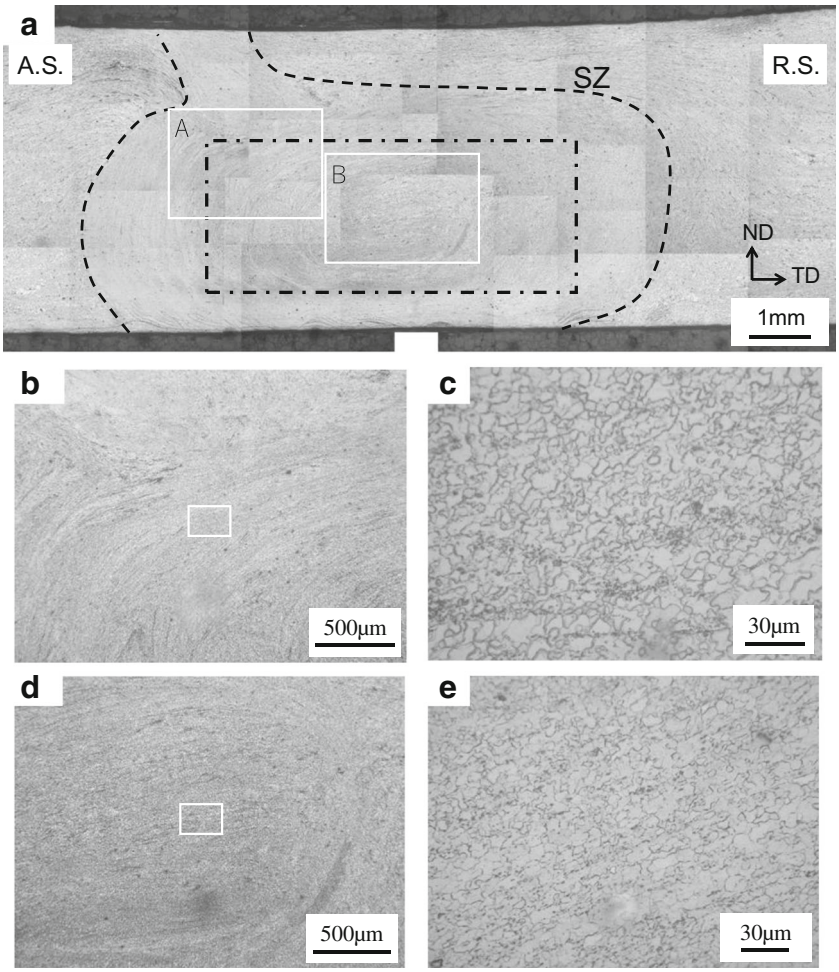

Fig. 4 Microstructures of the FSPed material: **a** Macroscopic view. **b** Magnified view of the area "A" in **a**. **c** Magnified view of the rectangular area in **b**. **d** Magnified view of the area "B" in **a**. **e** Magnified view of the rectangular area in **d**

process. Figure 3 shows the EDS analyses, in which Al-Ca-based IMCs are found as revealed in Fig. 3c, d. A large IMC shown by an arrow in Fig. 3a is identified as Al-Mn based one from Fig. 3c, e. The sizes of Al-Ca and Al-Mn-based IMCs are about a few μm and 60 μm, respectively. It is found that many small Al-Ca-based IMCs distribute densely, while the number of Al-Mn-based ones is quite limited. It has been reported that AMX602 consisted mainly of α-Mg grains, agglomerated Al-Ca-based IMCs, and a few Al-Mn ones, where Al-Ca and Al-Mn IMCs were identified as Al_2Ca and Al_6Mn or Al_8Mn_5, respectively [20]. Shen et al. [21] also mentioned that Al_2Ca fine particles existed in AMX602. The IMCs observed in the present work are also assumed to be such IMCs reported in the previous studies.

3.1.2 FSPed and FSP/aged materials

The macroscopic and detailed microstructures of the FSPed material observed on the cross-section perpendicular to the FSP direction are shown in Fig. 4. The side where the tool rotational direction corresponds to the tool traveling direction is denoted as AS (advancing side) and the other side as RS (retreating side). The stir zone (SZ) is seen within the broken line in the figure. The microstructure is apparently asymmetric between the AS and RS as shown in Fig. 4a. Elliptical onion-shaped structures [15] are seen in the square area indicated by the dash-and-dot line in Fig. 4a. This square area with the width of 6 mm and the height of 2.5 mm corresponds to the cross-section of the standard fatigue specimen (Fig. 1a) sampled from the SZ. Is should be noted that the fatigue specimens are sampled exactly from the severely-stirred and microstructurally-modified zone. The magnified views at the areas "A" and "B" in Fig. 4a are revealed in Fig. 4b, d, respectively, in which material flow is visible. Figure 4c, e is the magnified views of the rectangular areas in Fig. 4b, d, respectively. In the SZ, the grains are finer and IMCs distribute more uniformly than the as-received material. The average grain size in the SZ is 6.9 μm and finer than the as-received material (10.5 μm). The grain refinement is attributed to the dynamic recrystallization during FSP.

Figure 5 shows the EDS analyses of the FSPed material. The agglomeration of Al and Ca became further less than

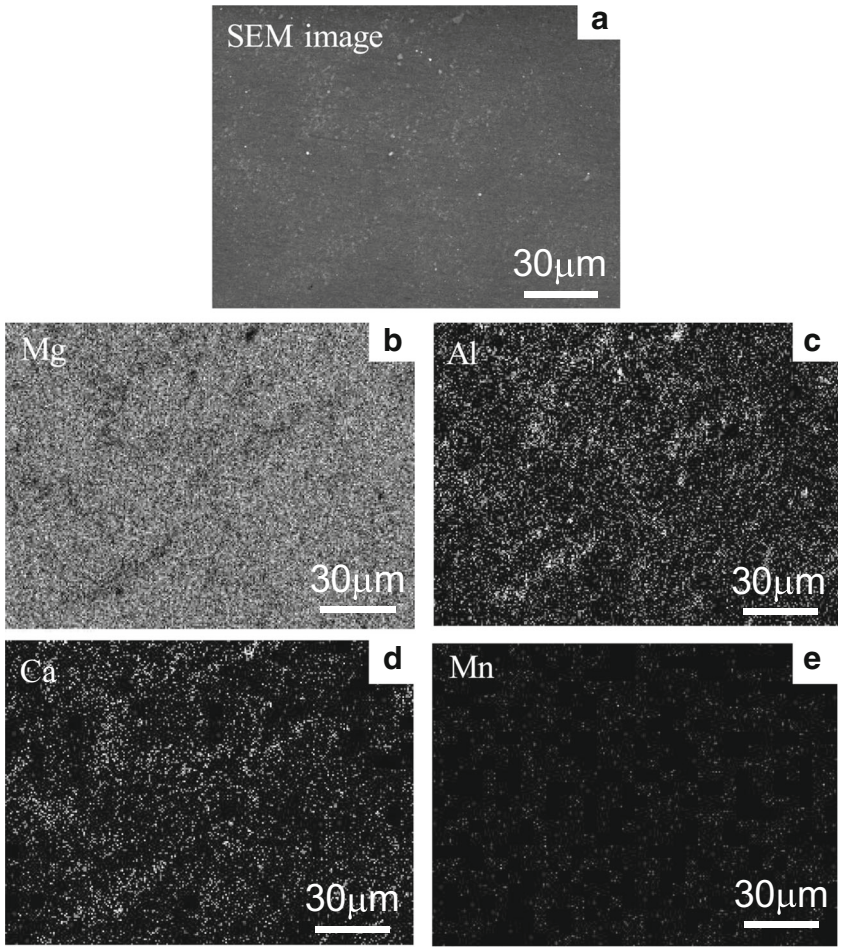

Fig. 5 SEM-EDS mapping of the FSPed material: **a** SEM image, **b** Mg, **c** Al, **d** Ca, **e** Mn

that in the as-received material (Fig. 3). It is considered that a part of Al-Ca-based IMCs was resolved into the matrix by heat input during FSP. Figure 6 also shows the EDS analyses of the FSPed material at the different location where some Al-Mn-based IMCs were detected. Comparing Fig. 6a with Fig. 3a, it is apparent that the size of Al-Mn-based IMC becomes smaller than that in the as-received material, which indicates that large Al-Mn-based IMCs were broken up by the stirring action of FSP. However, small Al-Mn-based IMCs were hardly detected in the microstructure. It can be summarized that FSP is effective to refine the microstructure, to resolve Al-Ca-based IMCs into the matrix and to break up large Al-Mn-based IMCs into small pieces. As for the aging process, the macroscopic and microscopic microstructures in the FSP/aged material were nearly the same with those of the FSPed one because the post-aging temperature (453 K) was not high enough to induce recrystallization and grain growth. Figure 7 shows the EDS analyses of the FSP/aged material observed near the center of the SZ. It can be seen that the sizes of both Al-Mn and Al-Ca-based IMCs are unchanged by the post-aging process.

3.2 Texture characterization

3.2.1 As-received material

Figure 8 shows the EBSD analyses on the cross-section, namely ND–TD plane, of the as-received material. The grains showing {10–10} plane (blue) and {2–1–10} plane (green) are frequently observed in Fig. 8a. On the other hand, the grains with (0001) plane (red) are hardly seen. Figure 8d shows the pole figures of (0001) and {10-10} planes. From these analyses, it is found that the texture is developed in the as-received material, where basal planes are nearly parallel to the RD. Similar texture was also reported by Park et al. [22] in AZ61 Mg alloy as the well-known hot-rolling texture of Mg alloys.

3.2.2 FSPed and FSP/aged materials

Figure 9 shows the texture analyses in the SZ of the FSPed material. The black broken line and dash-and-dot line in Fig. 9a indicate the SZ boundary and cross-

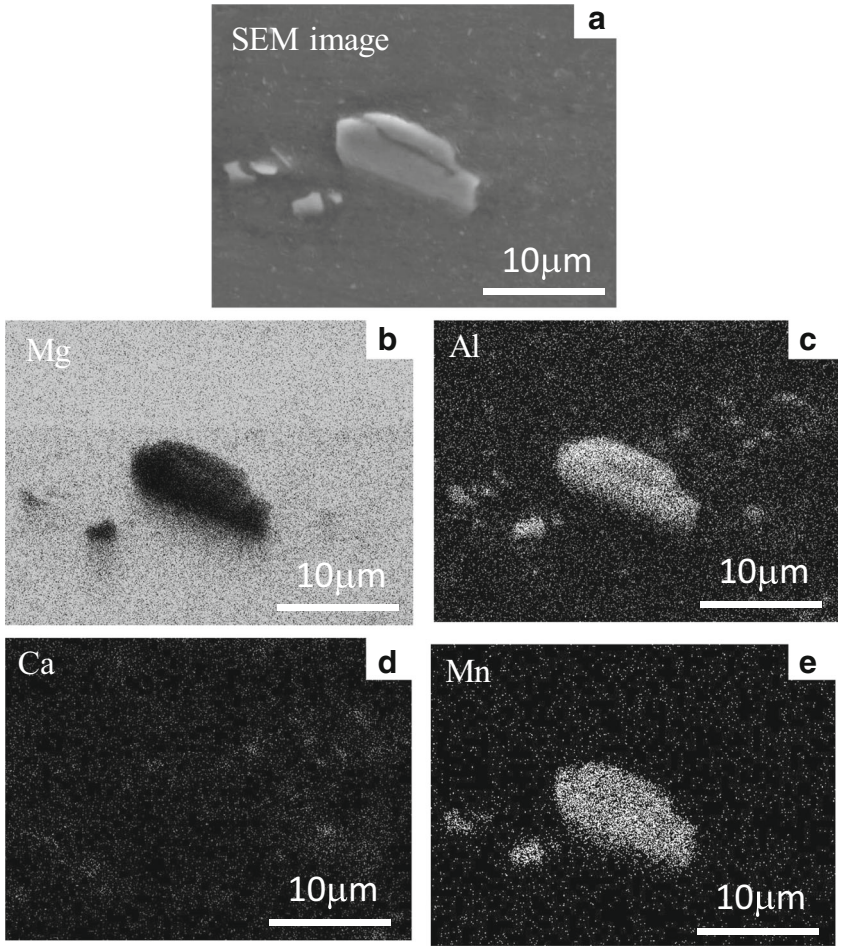

Fig. 6 SEM-EDS mapping of the FSPed material: **a** SEM image, **b** Mg, **c** Al, **d** Ca, **e** Mn

section of the standard specimen sampled from SZ, respectively. The EBSD analyses at the locations "A" (near the center of SZ) and at "B" (1.5 mm away from the center to RS) in Fig. 9a are shown in Fig. 9b, e, respectively. It is clear that the strong textures are formed at both locations. The IPF map at the center (Fig. 9b) reveals that (0001) planes are nearly perpendicular to the FSP direction. This result is similar with that by Park et al. [23]. They reported that *c*-axis was roughly perpendicular to the welding direction (WD) in the weld center region in the FSW joint of AZ61. In the RS (Fig. 9e), *c*-axis roughly has the angle of 45° to the FSP direction, which is also similar to the results by Park et al. [23]. This texture evolution is attributed to the shear plastic flow around the tool pin surface. It should be noted that the texture in the SZ of the FSPed material is stronger than that in the as-received one according to the pole figures (Figs. 8d, 9d, and h).

3.3 Mechanical properties

Figure 10 shows the hardness profiles of the FSPed and FSP/aged specimens, which were measured along the horizontal line at the mid thickness on the cross-section. The average hardness of the as-received material is 87 HV indicated by the solid line in the figure. In general, hardness increases with decreasing the grain size known as Hall-Petch effect of grain refinement. However, the hardness of the FSPed material is lower than that of the as-received one in the range of ± 6 mm from the center in spite of their finer grains. It is assumed that the as-received material was work hardened by the extrusion, while the heat input during FSP softened the matrix due to the decrease of dislocation density. Furthermore, AMX602 has age hardenability, thus heat input also resolved hardening precipitates into the matrix. It is noted that the hardness is slightly higher around the center of SZ, which is attributed to finer grains. The hardness increased by the post aging around ± 1~2 mm from the center, but still lower than the as-received material. Table 2 shows the tensile properties of the as-received and FSPed specimens. The proof stress and tensile strength of the as-received specimen are higher than those of the FSPed one while the elongations are the same. The lower tensile properties of the FSPed specimens correlate with the lower hardness.

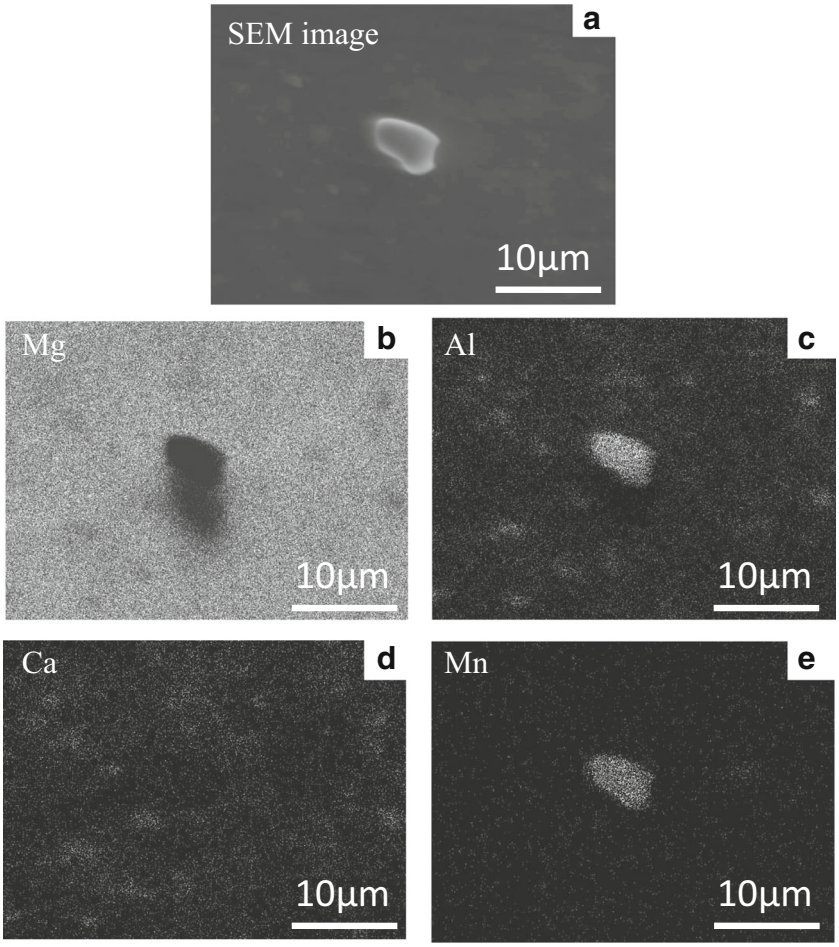

Fig. 7 SEM-EDS mapping of the FSP/aged material: **a** SEM image, **b** Mg, **c** Al, **d** Ca, **e** Mn

3.4 Fatigue properties

Figure 11 shows the *S-N* diagram, in which the fatigue limits are defined as the fatigue strengths at 10^7 cycles. The fatigue test results are summarized in Table 3. FSPes samples were tested at 70 and 60 MPa to check the detailed fatigue limits. The fatigue strengths of the FSPed and FSP/aged specimens are lower than those of the as-received ones, which indicates that FSP decreased fatigue strengths even though FSP successfully modified the microstructure from the viewpoints of grain refinement and uniform distribution of IMCs. Figure 12 indicates the typical fatigue fracture surfaces of the as-received, FSPed and FSP/aged specimens, where fatigue crack initiation sites show flat feature without inclusions. Figure 12e, f is Al and Ca mapping of Fig. 12d by EDS. The microstructural analyses revealed that IMCs were dispersed in the matrix. But IMC was not recognized at the crack initiation site as shown by Fig. 12d, e, f. It indicates that IMCs did not play an important role for fatigue crack initiation. The fatigue test results of the FSP/aged (gauge width 2 mm) specimens will be mentioned in the next section.

4 Discussion

The FSPed and FSP/aged specimens exhibited lower fatigue strengths than the as-received ones, even though the microstructure had been modified by FSP. As shown in Fig. 10, the hardness decreased after FSP, which could be related to the lower fatigue strengths. To investigate the effect of hardness on the fatigue strength, the detailed hardness distribution on the cross-section was measured. Figure 13 shows the fatigue crack initiation sites on the cross-sectional view with the contour map of hardness, in which crack initiation sites are indicated by the cross marks. The colored area corresponds to the cross-section of the fatigue specimen. It should be noted that the actual envelope of cross-section of fatigue specimen is shown by the solid line in Fig. 13a. The corners are curved by the surface polishing procedure as seen in Fig. 12g. In the map of the FSPed specimen (Fig. 13a), the fatigue cracks initiated near the sites where the hardness was nearly the minimum value of 62 HV. It should be noted that the average hardness of the as-received material is 87 HV

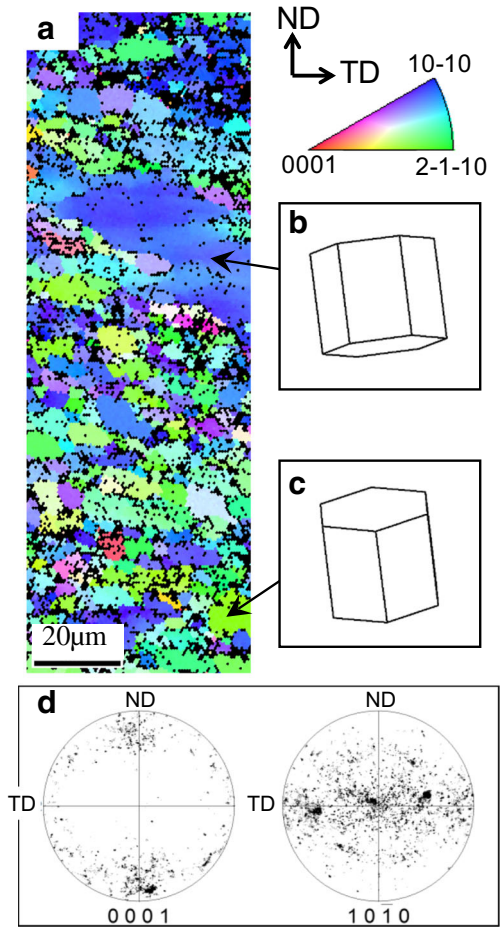

Fig. 8 EBSD analyses on the cross-section of the as-received material: **a** IPF map, **b**, **c** typical grain orientations, **d** pole figures of (0001) and (10–10) planes

and higher than that at the crack initiation sites. It is assumed that the low hardness is the predominant factor leading to the lower fatigue crack initiation resistance and lower fatigue strengths in the FSPed specimens. Figure 13b is the map of the FSP/aged specimen. It is apparent that the hardness increased by the post aging, while clear correlation between crack initiation sites and low hardness areas was not seen. For example, a fatigue crack initiated at the bottom side with higher hardness.

As described in Section 3.2, the FSPed material has stronger texture than the as-received one. HCP structure of Mg alloy has the strong anisotropy, where the critical resolved shear stress (CRSS) of the basal slip system is much lower than those of the other slip and twin systems. The material strengths and the deformation behavior could be affected by the angle between the loading direction and the texture orientation [23]. Therefore, textures also could be the factor leading to the lower fatigue strengths of the FSP/aged specimens. In the as-received material, the loading axis in the fatigue tests is parallel to the RD. Thus, the Schmid factors (SFs) of the basal slip systems were calculated for the typical grains shown in Fig. 8. The maximum SFs of the grains in Fig. 8b, c are 0.11 and 0.13, respectively, which are comparatively low. It indicates that the basal slip cannot operate easily under the fatigue loading. In the FSPed/aged specimens, the loading direction is parallel to the FSP direction. The maximum SFs of the typical grains on the RS shown in Fig. 9f, g are 0.45 and 0.49, respectively, which are comparatively higher. In the FSPed specimens, the texture could be dependent on the location. Subsequently, the detailed EBSD analyses are conducted to clarify how the textures distribute in the SZ. Figure 14 shows the pole figures of (0001) plane at the several sites "A" ~ "I" (Fig. 14a) on the cross-section. The cross-section of the fatigue specimen is also indicated by the white dash-and-dot line in the figure. At the locations "B" and "F" near the FSP tool center, the inclination of *c*-axis against FSP direction (fatigue loading direction) is small, while the inclination tends to increase in the AS and RS. It indicates that SFs of basal slips near the location "B" and "F" are smaller than the other locations in the AS and RS. The fatigue crack initiation sites of the FSP/aged specimens are not in the center but in the RS (Fig. 13b), where (0001) plane is inclined about 45° to the loading direction near the locations "C," "G," and "H." It indicates that the SFs of the basal slip are high and the basal slips could more easily operate, which resulted in the lower fatigue strengths of the FSP/aged specimens than the as-received ones. The FSP/aged specimens have higher hardness than the FSPed ones, and thus, the texture is a main factor for fatigue crack initiation. On the other hand, the lower hardness is the main factor in the FSPed specimens. It should be noted that the textures at the locations "A"~"I" are stronger than the texture of the as-received material (Fig. 8d).

The lower fatigue strengths of the FSPed and FSP/aged specimens than the as-received ones were attributed to the lower hardness and stronger texture. However, the core area of the FSP/aged material has the higher hardness and finer grains than the as-received material. Furthermore, SFs of basal slips tend to decrease near the core area as shown in Fig. 14. Therefore, the fatigue strengths might be increased or at least comparable to the as-received materials if the fatigue specimens are sampled from the core area of the SZ. In order to clarify the effects of hardness and texture of the FSP/aged material on the fatigue strengths, fatigue tests were performed using the specimens with a narrow gauge-section width of 2 mm as shown in Fig. 1b. The cross-section of the narrow-width specimen is also indicated in Fig. 14 by a white broken line. It should be

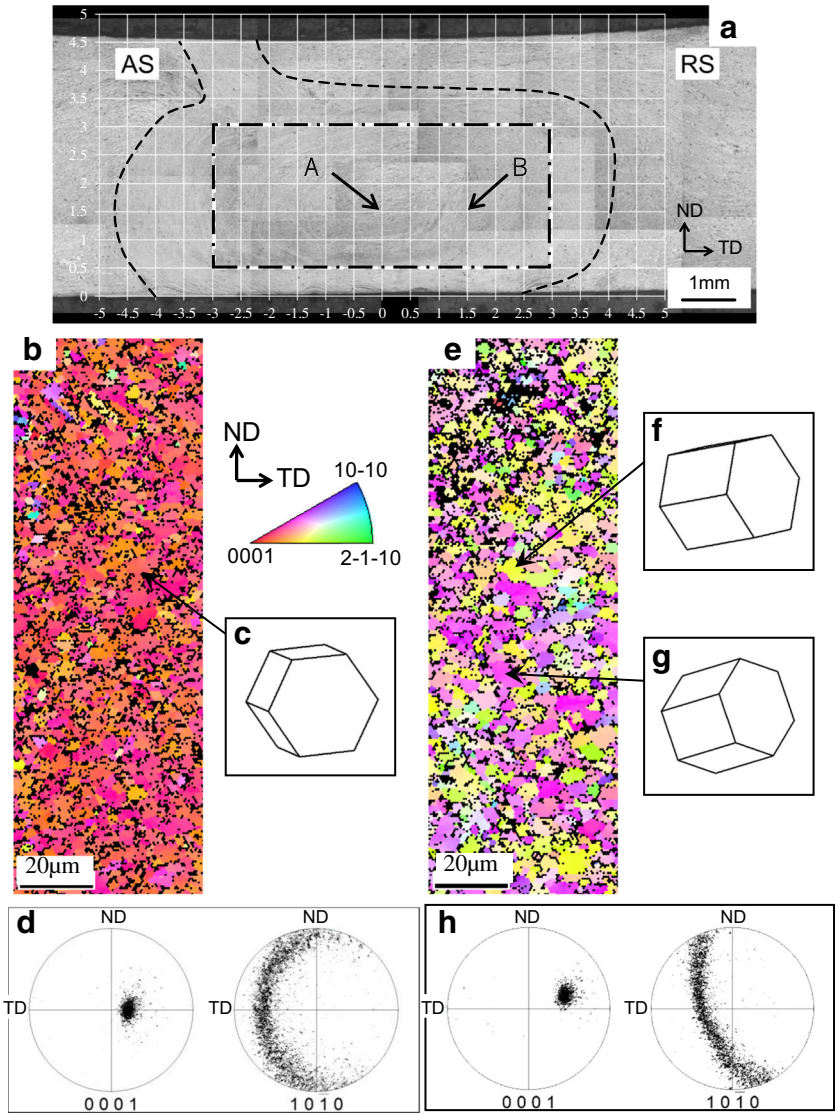

Fig. 9 EBSD analyses on the cross-section of the FSPed material: **a** Macroscopic appearance. **b**, **e** IPF maps at "A" and "B" in **a**, respectively. **c**, **f**, **g** Typical grain orientations. **d**, **h** Pole figures of (0001) and (10–10) planes

noted that the narrow gauge section corresponds to the core area of the SZ. These fatigue strengths of the core area of the SZ are plotted in Fig. 11 by solid symbols (shown as FSP/aged (gauge width 2 mm) in the figure). The fatigue strengths of the FSP/aged specimens with the width of 2 mm are higher than those of the FSPed and FSP/aged standard specimens, as expected. It means that the core area of the SZ has the higher fatigue strengths than the periphery of the SZ. The fatigue limit is comparable or slightly higher than the as-received specimen. Figure 15a shows the hardness distribution on the cross-section and fracture locations of the FSP/aged specimen with 2 mm width. Typical fatigue fracture surface and crack initiation site are revealed in Fig. 15b, c. The higher hardness and texture with lower SFs of basal slip are considered to be the factors leading to the increase of fatigue strengths of the FSP/aged specimens with a narrow gauge width. However, the fatigue strengths are nearly comparable to those of the as-received specimens. That is because the detrimental effect of the stronger texture on the fatigue performance still exists in the FSP/aged specimens, even if the specimens were sampled from the core area of the SZ.

In some early works [5–7], fatigue cracks initiated from large IMCs in flame-resistant Mg alloys. Masaki et al. [6] revealed that the size of round-shape inclusion at the crack initiations site was about 100 μm in diameter. However, due to the recent development of a casting technique of AMX602, such large IMC was hardly seen in the as-received microstructure, and IMC did not play important role in fatigue crack initiation. That is one of the reasons FSP could not enhance the fatigue strengths of the as-received material in the present study. However, from the viewpoint of mechanical

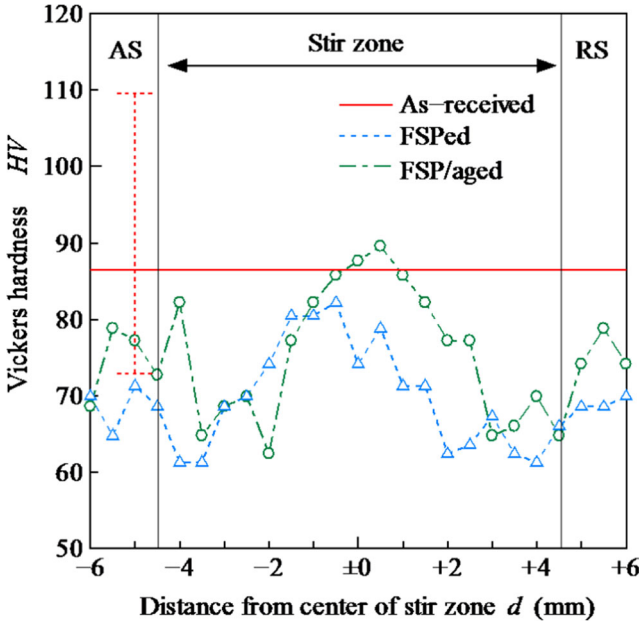

Fig. 10 Hardness profiles on the cross-section of FSPed and FSP/aged specimens

properties, it should be emphasized that the hardness of the core area of the SZ became higher than the as-received material by the post-aging process, and the fatigue limit of the core area was slightly higher than the as-received material. Furthermore, microstructure homogenization by FSP is beneficial for the as-received AMX602 with inhomogeneous distribution of IMCs.

5 Conclusions

Friction stir processing (FSP) was applied for the extruded Ca-added flame-resistant Mg alloy, AMX602, and the effects of FSP and post-aging treatment on the microstructure, texture, mechanical proprieties, and fatigue behavior were investigated. The main conclusions obtained can be made as follows:

1. The microstructure of the as-received AMX602 was successfully modified by FSP, where grain refinement, resolution of IMCs into the matrix and break up of large IMCs into small pieces occurred. On the other hand, the static mechanical properties decreased after FSP and the fatigue strengths also decreased. Post-aging heat treatment successfully increased the hardness of the FSPed material but could not increase the fatigue strengths to those of the as-received material.

Table 2 Mechanical properties of AMX602

Material	0.2% Proof stress $\sigma_{0.2}$ [MPa]	Tensile strength σ_2 [MPa]	Elongation [%]	Young's modulus E [GPa]
As-received	173	247	10	32
FSPed	80	199	10	30

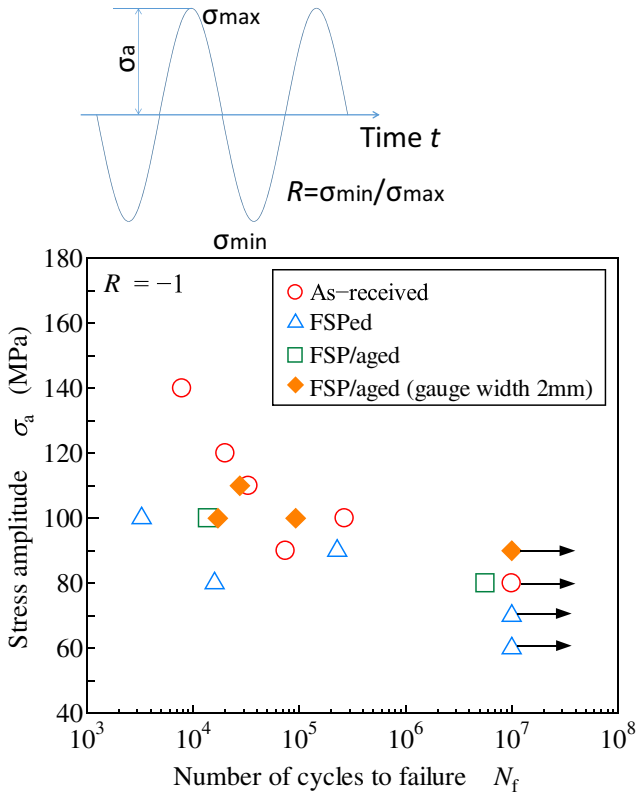

Fig. 11 *S-N* diagram

Table 3 Fatigue properties

Material	Stress amplitude σ_a [MPa]	Number of cycles to failure N_f	Stress amplitude σ_a [MPa]	Number of cycles to failure N_f
As-received	140	7870	100	266,880
	120	20,140	90	742,100
	110	33,190	80	> 10,000,000
FSPed	100	3280	70	> 10,000,000
	90	227,670	60	> 10,000,000
	80	15,960		
FSP/aged	100	13,800	80	5,655,200
FSP/aged	110	27,580	100	92,440
(gauge width 2 mm)	100	17,100	90	> 10,000,000

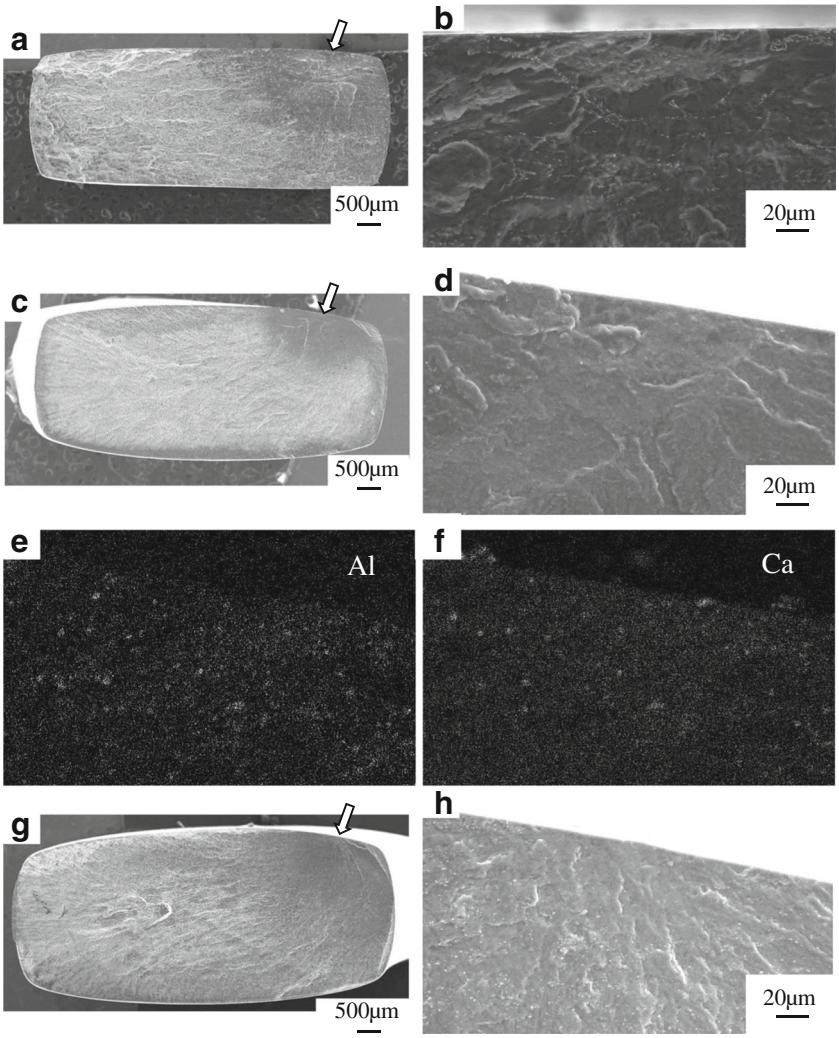

Fig. 12 SEM micrographs showing fatigue fracture surfaces near crack initiation sites: **a**, **b** As-received specimen (σ_a = 100 MPa, $N_f = 2.7 \times 10^5$). **c**, **d** FSPed specimen (σ_a = 100 MPa, $N_f = 3.3 \times 10^3$). **e** Al mapping of **d** by EDS. **f** Ca mapping of **d** by EDS. **g**, **h** FSP/aged specimen (σ_a = 100 MPa, $N_f = 1.4 \times 10^4$). Arrows indicate fatigue crack initiation sites. Right-hand figures are the magnified views at the crack initiation sites

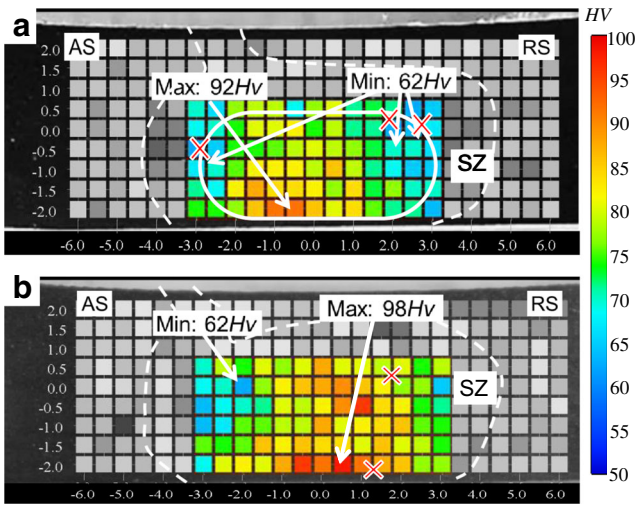

Fig. 13 Relationship between hardness distribution and crack initiation sites: **a** FSPed specimen, **b** FSP/aged specimen. Crosses indicate the fatigue crack initiation sites

2. The texture was found in the as-received plate depending on the extrusion process as that *c*-axis of HCP structure was aligned to the thickness direction. Textures changed by FSP as that *c*-axis was aligned to the FSP direction in the center and was inclined about 45° to the loading direction in the advancing and retreating sides.
3. Fatigue cracks of the FSPed specimens initiated at the locations where the hardness was minimal. The correlation between the crack initiation sites and local hardness was not clearly seen in the FSP/aged specimens, while cracks initiated at the locations with the strong texture, in which Schmid factor (SF) of the basal slip was high.
4. The fatigue strengths of the FSP/aged specimens were nearly the same with those of the as-receive ones when the test specimens were sampled as that the gauge section was included in the location where local hardness was comparable to the as-received material.

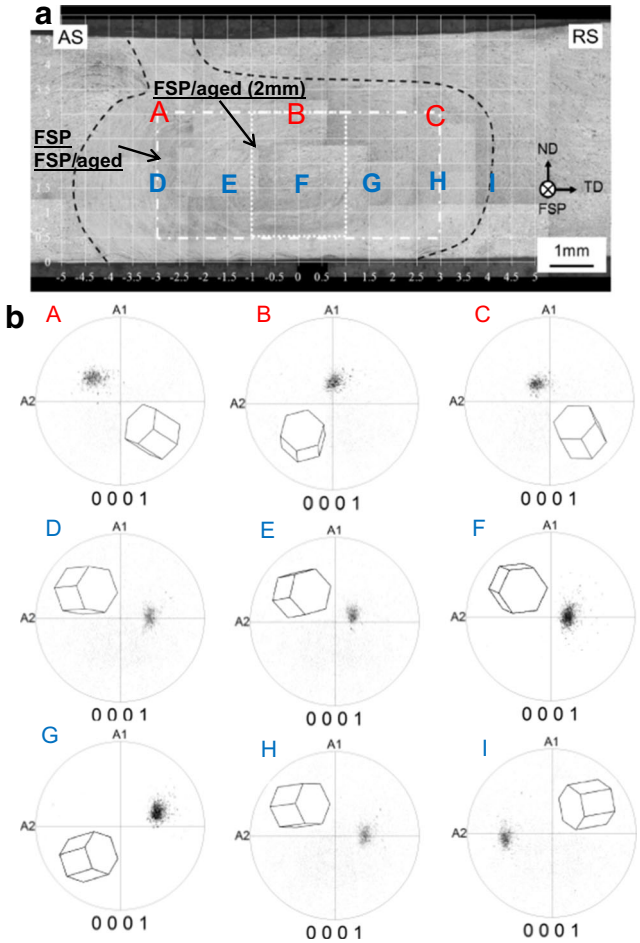

Fig. 14 Distribution of (0001) plane in the FSPed specimen: **a** Macroscopic appearance. **b** (0001) pole figures at the locations "A"~"I" in Fig. (a)

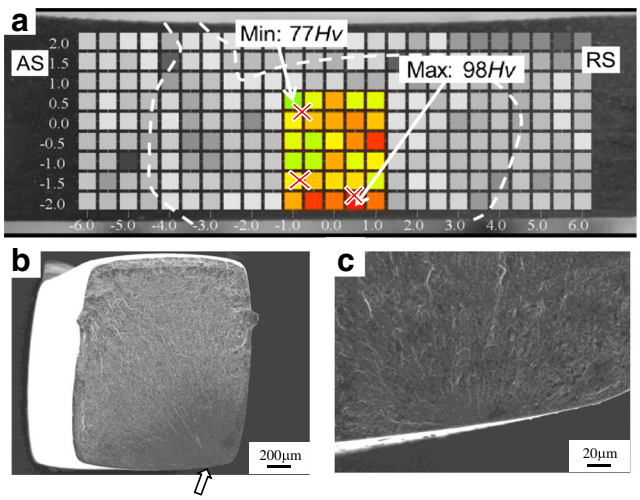

Fig. 15 Hardness distribution and crack initiation sites of the FSP/aged specimen (2 mm); **a** hardness distribution, **b** Fatigue fracture surface ($\sigma_a = 110$ MPa, $N_f = 2.8 \times 10^4$), **c** magnified view at the crack initiation site. The arrow in **b** indicates the crack initiation site

References

1. Kulekci MK (2008) Magnesium and its alloys applications in automotive industry. Int J Adv Manuf Technol 39(9-10):851–865. https://doi.org/10.1007/s00170-007-1279-2
2. Sakamoto M, Akiyama S, Ogi K (1997) Suppression of ignition and burning of molten Mg alloys by Ca bearing stable oxide film. J Mater Sci Lett 16(12):1048–1050. https://doi.org/10.1023/A:1018526708423
3. Hakamada M, Watazua A, Saito N, Iwasaki H (2010) Dynamic recrystallization during hot compression of as-cast and homogenized noncombustible Mg–9Al–1Zn–1Ca (in mass%) alloys. Mater Sci Eng A 527(26):7143–7146. https://doi.org/10.1016/j.msea.2010.07.084
4. Watanabe H, Yamaguchi M, Takigawa Y, Higashi K (2007) Mechanical properties of Mg–Al–Ca alloy processed by hot extrusion. Mater Sci Eng A 454-455:384–388. https://doi.org/10.1016/j.msea.2006.12.130
5. Kitahara Y, Ikeda K, Shimazaki H, Noguchi H, Sakamoto M, Ueno H (2006) Fatigue strength characteristics of non-combustible Mg alloy. Trans Jpn Soc Mech Eng Series A 72(717):661–668 **(in Japanese)**. https://doi.org/10.1299/kikaia.72.661
6. Masaki K, Ochi Y, Kakiuchi T, Kurata K, Hirasawa T, Matsumura T, Takigawa Y, Higashi K (2008) High cycle fatigue property of extruded non-combustible Mg alloy AMCa602. Mater Trans 49(5):1148–1156. https://doi.org/10.2320/matertrans.MC2007108
7. Sakai T, Kikuchi S, Nakamura Y, Ninomiya N (2015) A study on very high cycle fatigue properties of low flammability magnesium alloy in rotating bending and axial loading. App Mech Mater 782:27–41
8. Kulekci MK, Esme U, Buldum B (2016) Critical analysis of friction stir-based manufacturing processes. Int J Adv Manuf Technol 85(5-8):1687–1712. https://doi.org/10.1007/s00170-015-8071-5
9. Mishra RS, Mahoney MW, McFadden SX, Mara NA, Mukherjee AK (2000) High strain rate superplasticity in a friction stir processed 7075 Al alloy. Scripta Mater 42:163–168
10. Ma ZY, Sharma SR, Mishra RS (2006) Effect of friction stir processing on the microstructure of cast A356 aluminum. Mater Sci Eng A 433(1-2):269–278. https://doi.org/10.1016/j.msea.2006.06.099
11. Jana S, Mishra RS, Baumann JA, Grant G (2010) Effect of process parameters on abnormal grain growth during friction stir processing of a cast Al alloy. Mater Sci Eng A 528(1):189–199. https://doi.org/10.1016/j.msea.2010.08.049
12. Tajiri A, Uematsu Y, Kakiuchi T, Tozaki Y, Suzuki Y, Afrinaldi A (2015) Effect of friction stir processing conditions on fatigue behavior and texture development in A356-T6 cast aluminum alloy. Int J Fatigue 80:192–202. https://doi.org/10.1016/j.ijfatigue.2015.06.001
13. Chang CI, Lee CJ, Huang JC (2004) Relationship between grain size and Zener–Holloman parameter during friction stir processing in AZ31 Mg alloys. Scripta Mater 51(6):509–514. https://doi.org/10.1016/j.scriptamat.2004.05.043
14. Tsujikawa M, Chung SW, Tanaka M, Takigawa Y, Oki S, Higashi K (2005) High-strengthening of Mg–5.5 mass%Y–4.3 mass%Zn cast alloy by friction stir processing. Mater Trans 46(12):3081–3084. https://doi.org/10.2320/matertrans.46.3081
15. Uematsu Y, Tokaji K, Fujiwara K, Tozaki Y, Shibata H (2009) Fatigue behaviour of cast magnesium alloy AZ91 microstructurally modified by friction stir processing. Fat Frac Engng Mater Struct 32(7):541–551. https://doi.org/10.1111/j.1460-2695.2009.01358.x
16. Mohan A, Yuan W, Mishra RS (2013) High strain rate superplasticity in friction stir processed ultrafine grained Mg–Al–Zn alloys.

Mater Sci Eng A 562:69–76. https://doi.org/10.1016/j.msea.2012.11.026

17. Woo W, Choo H, Brown DW, Liaw PK, Feng Z (2006) Texture variation and its influence on the tensile behavior of a friction-stir processed magnesium alloy. Scripta Mater 54(11):1859–1864. https://doi.org/10.1016/j.scriptamat.2006.02.019
18. Chena J, Fujii H, Sun Y, Morisada Y, Kondoh K, Hashimoto K (2012) Effect of grain size on the microstructure and mechanical properties of friction stir welded non-combustive magnesium alloys. Mater Sci Eng A 549:176–184. https://doi.org/10.1016/j.msea.2012.04.030
19. Liu FC, Ma ZY, Tan MJ (2013) Facilitating basal slip to increase deformation ability in Mg-Mn-Ce alloy by textural reconstruction using friction stir processing. Metall Mater Trans A 44(8):3947–3960. https://doi.org/10.1007/s11661-013-1746-3
20. Liao J, Hotta M (2015) Atmospheric corrosion behavior of field-exposed magnesium alloys: influences of chemical composition and microstructure. Corr Sci 100:353–364. https://doi.org/10.1016/j.corsci.2015.08.021
21. Shen J, Kondoh K, Jones TL, Mathaudhu SN, Kecskes LJ, Wei Q (2016) Effect of strain rate on the mechanical properties of magnesium alloy AMX602. Mater Sci Eng A 649:338–348. https://doi.org/10.1016/j.msea.2015.10.022
22. Park SHC, Sato YS, Kokawa H (2003) Basal plane texture and flow pattern in friction stir weld of a magnesium alloy. Metall Mater Trans A 34(4):987–994. https://doi.org/10.1007/s11661-003-0228-4
23. Park SHC, Sato YS, Kokawa H (2003) Effect of micro-texture on fracture location in friction stir weld of Mg alloy AZ61 during tensile test. Scripta Mater 49(2):161–166. https://doi.org/10.1016/S1359-6462(03)00210-0